science, engineering and health studies

Research Article

Science, Engineering and Health Studies
https://lio1.tci-thaijo.org/index.php/sehs
ISSN (Online): 2630-0087

Deconvolution strategies for spatial localization of β-catenin protein

Reetoja Nag[1], Aparajita Karmakar[2], Chris Ngan[3], Noel Whitaker[3], Priyanka Srivastava[4], and Raunak Kumar Das[1,3]*

[1] Centre for Biomaterials Cellular and Molecular Theranostics, Vellore Institute of Technology, Tamilnadu 632014, India
[2] School of Information Technology and Engineering, Vellore Institute of Technology, Tamilnadu 632014, India
[3] School of Biotechnology and Biomolecular Sciences, University of New South Wales, Sydney 2052, Australia
[4] Centre for Nanobiotechnology, Vellore Institute of Technology, Tamilnadu 632014, India

***Corresponding author**:
Raunak Kumar Das
raunakkumardas@vit.ac.in

***Received**: 3 April 2025*
***Revised**: 14 August 2025*
***Accepted**: 14 September 2025*
***Published**: 6 November 2026*

***Citation**:
Nag, R., Karmakar, A., Ngan, C., Whitaker, N., Srivastava, P., & Kumar Das, R. (2026). Deconvolution strategies for spatial localization of β-catenin protein. Science, Engineering and Health Studies, 20, 26040007.*

ABSTRACT

Wide field fluorescence microscopes (WFFM) are widely used due to their affordability and ease of use, but they suffer from a significant limitation: the images often appear blurry because light from above and below the focal plane contributes to the final image. Eliminating this out-of-focus light typically requires expensive equipment like confocal microscopes. This study aimed to address this issue by applying deconvolution algorithms to images obtained from conventional WFFM. MATLAB was used to implement adaptive histogram equalization, unsharp masking, and thresholding operations, while the Lucy Richardson algorithm was applied in Python. Both approaches successfully removed out-of-focus blur and enabled quantification of the percentage of β-catenin expression overlapping with nuclei at 0, 36, and 48 h post transfection of C33A cell lines with HPV16 & 18 E6/E7 oncogenes. Our results indicated that deconvoluted images revealed a higher percentage of β-catenin overlapping the nuclei compared to non-deconvoluted images: for example, in MATLAB, 13.63% vs. 9.23% at 0 h, 15.55% vs. 11.26% at 36 h, and 18.33% vs. 12.55% at 48 h. In Python, similar trends were observed, with the control showing 1.29% vs. 0.54%. This method is a computationally efficient and cost-effective solution for removing out-of-focus light from WFFM images, making it particularly useful for institutions with limited access to high-cost microscopy equipment.

Keywords: deconvolution; fluorescence microscopy; β-catenin

1. INTRODUCTION

Fluorescence microscopy has become an indispensable tool for studying cellular physiology, thanks to the availability of a variety of customizable fluorescent dyes that specifically target proteins, lipids, or ions (Hickey et al., 2022). The efficiency of this technique is further enhanced by the optical filter sets in modern microscopes, which allow researchers to visualize the fluorescent signals by harnessing the excitation and emission spectra of these dyes (Grimm & Lavis, 2022). Wide-field fluorescence microscopes (WFFM) are among the most widely used systems in laboratories due to their versatility and accessibility (Shi et al., 2019). However, despite their popularity, conventional WFFMs suffer from significant limitations.

One of the primary drawbacks of traditional WFFMs is the presence of out-of-focus light, which results in blurred images and lowers contrast. This blurring arises from light originating in planes above and below the focal plane, leading to potential misinterpretation of the signals obtained (Pushpa et al., 2023). Consequently, the images produced by WFFMs often lack the spatial resolution necessary for accurate analysis, rendering them less

suitable for certain applications. This limitation has spurred interest in more advanced imaging techniques such as confocal and super-resolution microscopy.

Confocal microscopy provides optical sectioning by removing out-of-focus light, offering clearer and more detailed images. However, this method has limitations, particularly when imaging deeper into thicker samples, where spherical aberrations hinder light penetration (Wu & Hammer, 2021). Super-resolution microscopy, which surpasses the diffraction limit, provides even higher resolution, but it often requires the combination of other techniques, such as two-photon microscopy, to image larger volumes and deeper structures effectively (Valli et al., 2021). Furthermore, the prohibitive cost of acquiring and maintaining confocal and super-resolution microscopes restricts their use to specialized facilities, making them inaccessible to many laboratories (Wu et al., 2021). Additionally, practical constraints, such as signal-to-noise ratio, optical aberrations, and sampling rates, can limit the resolution achievable in real-world applications (Lambert & Waters, 2017).

In this context, deconvolution techniques offer a cost-effective alternative to improve the quality of WFFM images. Deconvolution algorithms correct image blurring by reassigning out-of-focus light to its proper location in the focal plane, enhancing image clarity and contrast. These algorithms fall into two main categories: deblurring algorithms and restoration (deconvolution) algorithms (Yadav et al., 2016). Deblurring algorithms, such as nearest-neighbor and multi-neighbor approaches, are computationally simpler but suffer from reduced signal-to-noise ratios and the potential introduction of artifacts (Kaur & Kaur, 2016; Satish et al., 2020). In contrast, deconvolution algorithms handle blur as a three-dimensional problem, yielding superior image quality by convolving the image data with the point spread function (PSF) of the imaging system (Lau et al., 2023).

Among deconvolution algorithms, techniques such as Wiener deconvolution, regularized least squares, and Lucy Richardson deconvolution stand out (Hasan, 2016; He et al., 2021). While these methods can produce high-quality images, they may also amplify noise, introduce ringing artifacts, or result in some loss of image detail. Nonetheless, recent developments in open-source software have made deconvolution more accessible to researchers. For instance, the MATLAB toolbox DVDeconv includes algorithms that account for depth asymmetry in PSFs (Kim, 2021). ImageJ also offers deconvolution plugins like DeconvolutionLab2, Ops deconvolution, and Iterative Deconvolve 3D, though these often require image-specific parameter adjustments (Schneider et al., 2012; Sage et al., 2017; Pietzsch et al., 2012; Bruce & Butte, 2013).

Despite these advancements, it remains a need for a generalized deconvolution algorithm that can adapt to different image contrasts and equalize luminosity across varying inputs. In the present study, the nuclear accumulation of β-catenin, a critical marker in cancer progression, was investigated using WFFM. To enhance the clarity of these images, cost-effective deconvolution algorithms were applied, including adaptive histogram equalization, unsharp masking, and Lucy Richardson deconvolution, implemented in MATLAB 2016b and Python 3.7 (with scikit-image, OpenCV, NumPy, and Matplotlib libraries). By optimizing these algorithms, we aimed to provide an accessible and computationally efficient solution for improving image quality in fluorescence microscopy. This approach highlights the potential of deconvolution techniques as a viable alternative for researchers who may not have access to more advanced and costly imaging systems.

2. MATERIALS AND METHODS

2.1 Cell lines and culture

C-33A (cervical cancer cell line devoid of HPV was transfected with pLXSN containing HPV16 E6/E7 by the use of Lipofectamine LTX PLUS reagent (pLXSN:Lipofectamin LTX:PLUS) in the ratio of 2:4:2.

2.2 Immunocytochemistry

The expression of the HPV16 & 18 E6/E7 oncogenes in cells were screened with appropriate primers targeting E6 and E7. Cells grown on coverslips were analyzed for β-catenin by immunocytochemistry (Chakraborti et al., 2023). Alexa Fluor 594 was the dye used for visualizing β-catenin, which was then counterstained with DAPI, the dye used for visualizing nuclei (Chakraborti et al., 2023).

2.3 Imaging

The WFFM images at 0, 36, and 48 h were captured by Olympus FSX100 microscope equipped with a UPlanSApo 40x/0.95 numerical aperture (NA) Plan-Apochromat objective. Imaging was performed using three filters: ultraviolet (360–370 nm), blue (460–495 nm), and green (530–550 nm). The images were digitally captured with a CCD camera (pixel size 6.0 µm × 6.0 µm; resolution: 1360 × 1024 pixels) with a maximum resolution of 12.5 megapixels. Metal halide fluorescence light source was used for illumination.

2.4 Deconvolution of fluorescence microscopic images and β-catenin nuclei percentage calculation in MATLAB and Python

The fluorescence microscopic images of β-catenin and nuclei were captured for control, 36 h, and 48 h and the methodology was applied for 5 images per time point.

2.4.1 MATLAB process

The images were separated into single-channel images—blue for nuclei and red for β-catenin. Deconvolution was performed using adaptive histogram equalization and unsharp masking in MATLAB 2016b (Sidhu et al., 2023; Khan et al., 2020; Kumar et al., 2022; Kanthan & Sujatha, 2016). In our methodology, adaptive histogram equalization method, which uses a kernel size of 21*21, enhances contrast by dividing the image into small tiles. It improves contrast in areas that are brighter or dimmer than the rest. After that, in unsharp masking, a blurred, negative image (the "unsharp" mask) is added to the original image, producing a sharper image. After deconvolution of the individual nuclei and β-catenin images, they are combined to calculate the percentage of β-catenin inside the nuclei. The non-deconvoluted images are also processed for comparison. Thresholding with a threshold limit of 100 pixels is performed to exclude red pixels outside the nuclei. The percentage of β-catenin inside the nuclei was calculated using Equation 1:

$$\%\ of\ \beta\ catenin\ in\ nuclei = No.of\ red\ pixels / No.of\ blue\ pixels\ x\ 100 \quad (1)$$

2.4.2 Python process

Similarly, deconvolution and analysis were done using Python for single-channel blue and red fluorescent microscopic images. Adaptive histogram equalization was applied to blue and red channel images. A kernel size of 1/8 of the image dimensions was used for nuclei images, and a larger kernel size of 20 was applied for β-catenin images. After that, Lucy Richardson deconvolution iterative method was applied to the red channel images with a 5x5 PSF and 30 iterations to minimize over-estimation and reduce computation time (Hojjatoleslami et al., 2013; Bai et al., 2022). After deconvolution, thresholding was applied as follows: If the 90th percentile of the image's pixel values was less than 100, the threshold was set to 100 to avoid using too low a threshold, otherwise, the threshold was set to the 90th percentile value. Both red and blue images were thresholded to isolate pixels for further analysis. The percentage of β-catenin inside the nuclei was calculated using Equation 2:

$$\%\ of\ \beta\ catenin\ in\ nuclei = \frac{\Sigma\left(\frac{red\ pixels\ above\ threshold \wedge blue\ pixels\ above\ threshold}{Total\ no.of\ blue\ pixels\ above\ threshold}\right)}{number\ of images\ in\ the\ group} \times 100 \qquad (2)$$

3. RESULTS

Analysis using MATLAB depicted clear and crisp expression of β-catenin in the deconvoluted images at various timepoints post transfection (Figure 1 B2, E2, and H2). Immediately after transfection, β-catenin expression was observed around the blue nuclei (Figure 1 C1 and C2). By 36 and 48 h post-transfection (Figures 1 E1, E2, F1, F2, H1, H2, I1, and I2), β-catenin expression increased and was distributed throughout the nucleus. Thresholded deconvoluted images (Figure 2) revealed higher β-catenin levels inside nuclei over time. The Python analysis results (Figure 3) showed the thresholded red channel images demonstrating β-catenin nuclear accumulation. In addition, Figure 4 outlines the image processing steps used in the pipeline. Despite slight variations, deconvolution improved β-catenin quantification accuracy across time points. Both MATLAB (Figure 1) and Python (Figure 3) analysis visually indicated increased β-catenin overlap with nuclei at 36 and 48 h compared to control.

The percentage of β-catenin inside nuclei for different time points for original and deconvoluted images, as calculated by MATLAB is shown in Table 1. The percentage of β-catenin inside nuclei for different time points for original and deconvoluted images, as calculated by Python programming is shown in Table 2. Both methods, after deconvolution, depicted a greater number of red pixels overlapping the blue pixels in images obtained at 36 and 48 h post transfection compared to the control immediately after transfection (Figure 1 F2 and I2 for MATLAB; Figure 3 D and F Python). This signifies that there is greater nuclear accumulation of β-catenin post 36 and 48 h transfection. Moreover, the calculated percentage accumulation of β-catenin in the nuclei for the different time points in the deconvoluted images were found to be more in comparison to those in the non-deconvoluted images in analysis via MATLAB (Table 1), (9.2389%, 11.2669%, and 12.5506% for 0, 36, and 48 h for non-deconvoluted images and 13.6321%, 15.5556%, and 18.3353% for 0, 36, and 48 h for deconvoluted images) showing that as a result of better resolution, the accumulation of β-catenin is better visualized and calculated. For analysis via Python (Table 2), we can see an increase in the percentage of β-catenin inside the nuclei as compared to the control, both before and after the deconvolution corrected images. However, by implementing deconvolution, we see our percentages are slightly lower for 36 (17.5901% for non-deconvoluted and 16.2737% for deconvoluted images) and 48 h (12.9185% for non-deconvoluted and 12.6536% for deconvoluted images) whereas it has increased for control images (0.5446% for non-deconvoluted and 1.2996% for deconvoluted images). The percentage of β-catenin inside the nucleus increased with progression of time, however, the reduction in β-catenin from 36 to 48 h could be due to change of intensity of β-catenin as it spreads within the nucleus (as calculated in both the raw and deconvoluted images).

Table 1. Percentage of β-catenin inside nuclei for different time durations in original and deconvoluted images, as calculated by MATLAB

S. No.	Time duration	Percentage of β-catenin inside nuclei for original images	Percentage of β-catenin inside nuclei for deconvoluted images
1	0 h	9.2389%	13.6321%
2	36 h	11.2669%	15.5556%
3	48 h	12.5506%	18.3353%

Table 2. Percentage of β-catenin inside nuclei for different time durations in original and deconvoluted images, as calculated by Python

Sl. No.	Time duration	Percentage of β-catenin inside nuclei for original images	Percentage of β-catenin inside nuclei for deconvoluted images
1	0 h	0.5446%	1.2996%
2	36 h	17.5901%	16.2737%
3	48 h	12.9185%	12.6536%

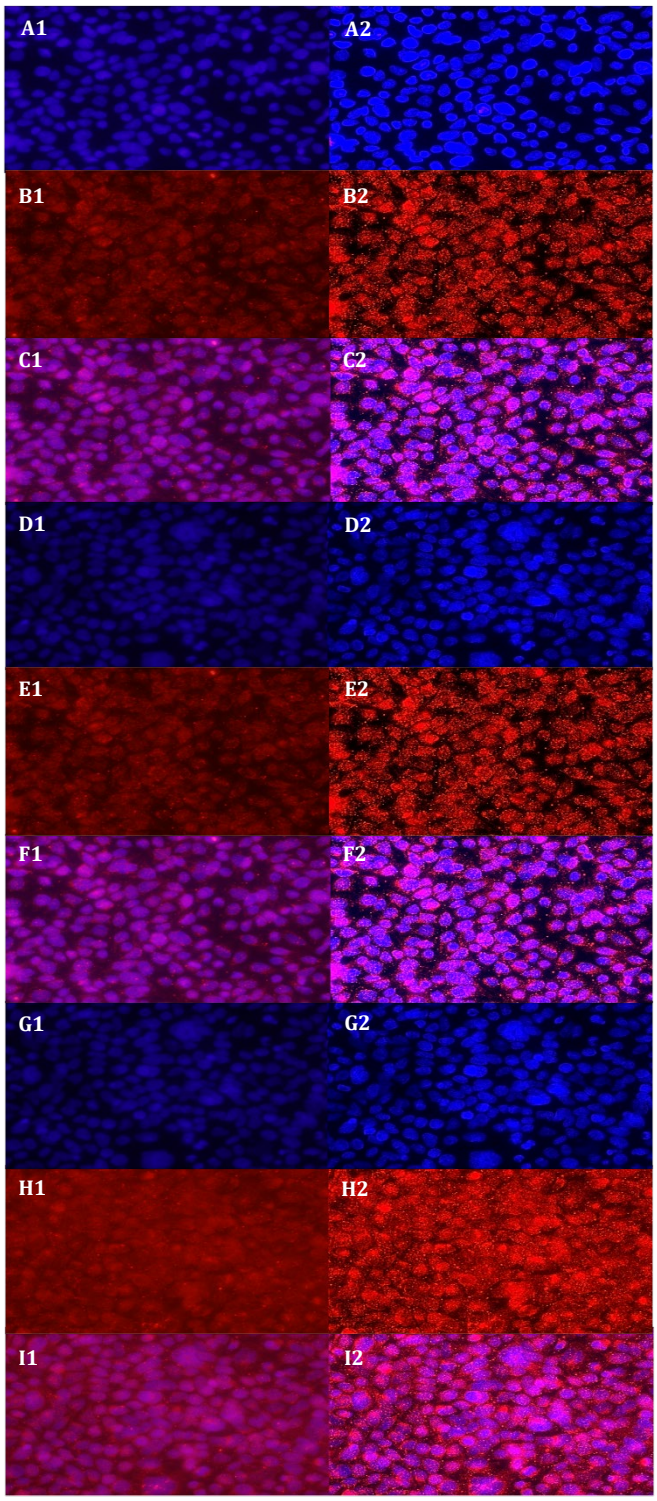


Figure 1. Increases in nuclear accumulation of β-catenin

A1 to C2 represents images taken immediately after transfection, D1 to F2 36 h after transfection, and G1 to I2 48 h after transfection. A1, B1, and C1 depict the original images of dapi stained nucleus, β-catenin and merged image of dapi stained nucleus, and β-catenin respectively. Similarly, A2, B2, and C2 represent the deconvoluted images of the dapi stained nucleus, β-catenin, and merged image of dapi stained nucleus and β-catenin respectively. A similar method has been followed to depict the images of 36 and 48 h post transfection in images from D1 to I2.

The deconvoluted images by analysis using MATLAB showed a greater increase in β-catenin percentage in nuclei across the time points in comparison to the original images. The pixels were better visualized and counted in the deconvoluted images, as they had better contrast than the original ones.

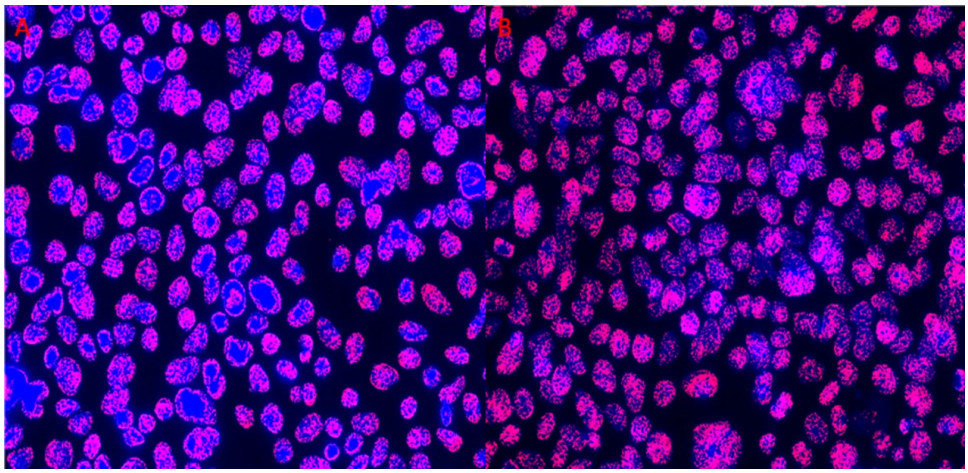


Figure 2. Accumulation of β-catenin inside nuclei during (A) 36 h and (B) 48 h.

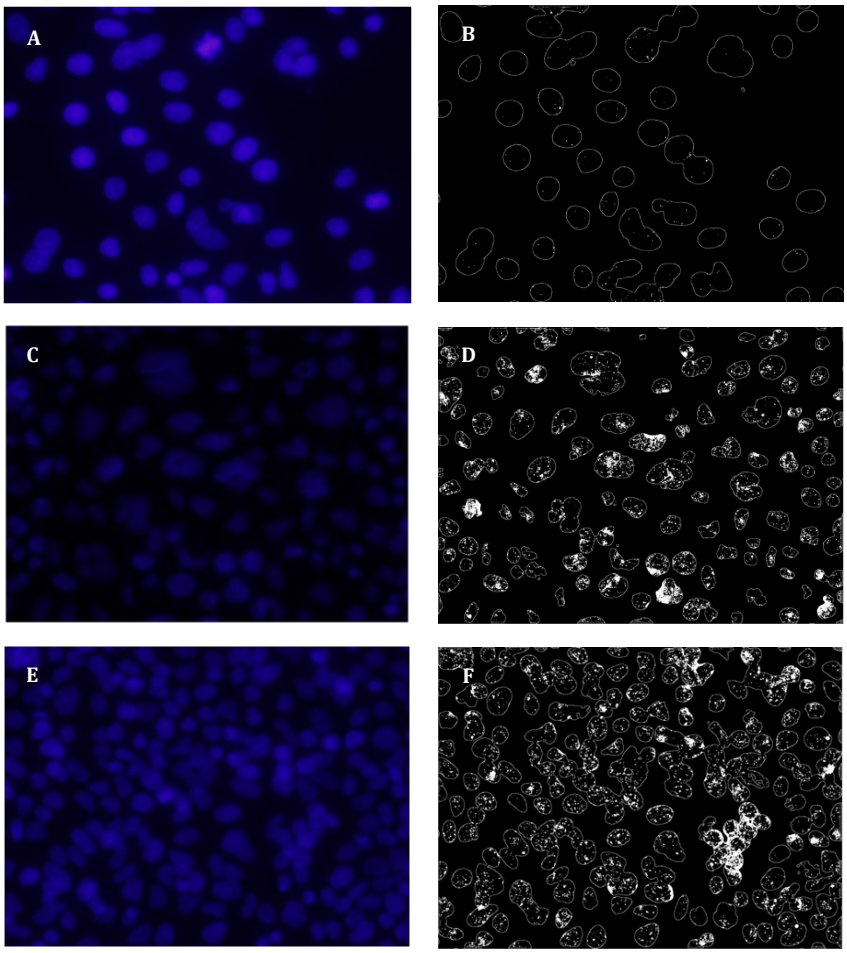


Figure 3. (A) 0 h original nuclei image, (B) 0 h nuclei contours superimposed on thresholded β-catenin showing very little β-catenin accumulation inside the nucleus, (C) 36 h original nuclei image, (D) 36 h nuclei contours superimposed on thresholded β-catenin showing β-catenin starts to accumulate inside the nucleus, (E) 48 h original nuclei image, (F) 48 h nuclei contours superimposed on thresholded β-catenin showing further progress of β-catenin inside the nucleus

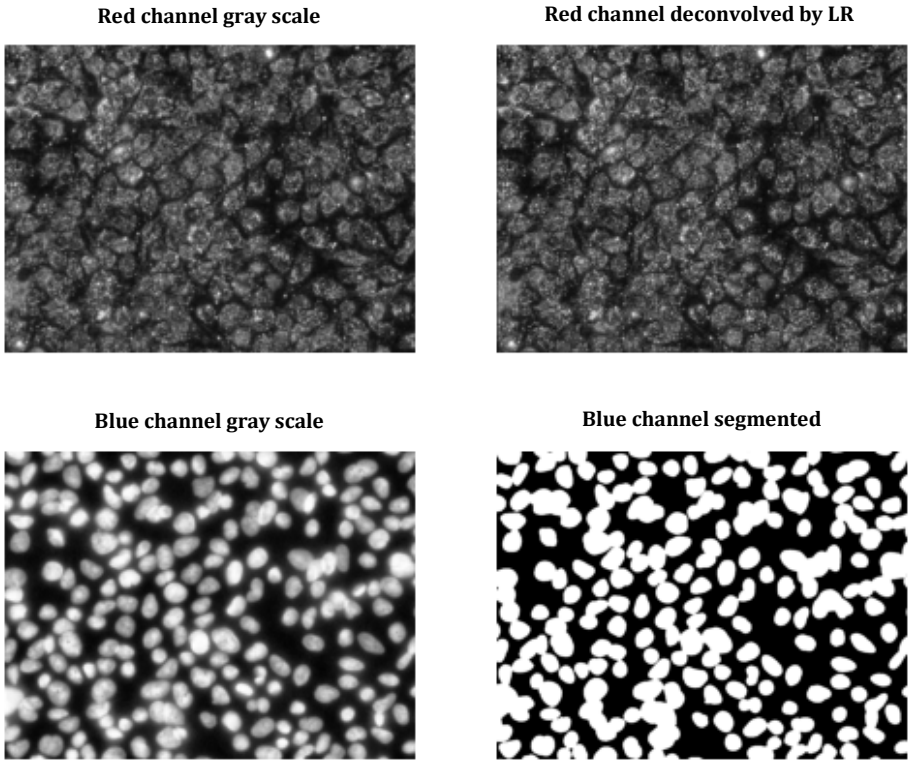


Figure 4. The image processing techniques implemented on the images via Python (image from the 36 h group)

Figure 4 shows the enhancement of red channel image by Lucy Richardson (LR) and nuclei segmentation from the blue channel images.

4. DISCUSSION

β-catenin plays a pivotal role in cell adhesion and migration, and its aberrant behavior is closely linked to cancer progression (Kaszak et al., 2020). The subcellular localization of β-catenin serves as a key marker of this process (Kaszak et al., 2020). Specifically, cytoplasmic accumulation followed by nuclear translocation of β-catenin is a hallmark of the Wnt signaling pathway, a process often associated with tumorigenesis and cancer progression, including colorectal and other cancers (Disoma et al., 2022). Nuclear localization of β-catenin, a critical indicator of malignant transformation, has been widely documented in various tumor types (Xu et al., 2019; Perrone et al., 2014). Additionally, reduced β-catenin expression at the cell membrane is frequently correlated with metastatic potential in malignant tumors (Ramos-García & González-Moles, 2022). In our study, we observed an increase in β-catenin's nuclear accumulation over time in cervical cell lines, with high-resolution deconvoluted images revealing this progression; thus it reinforces its role as a marker of cancer development.

Among the deconvolution techniques tested, Lucy Richardson deconvolution yielded the most effective results, outperforming alternatives such as Wiener, unsupervised Wiener, and unwrap phase inverse filters. Lucy Richardson's superior performance was attributed to its ability to provide a good estimate of the PSF within a manageable number of iterations, offering improved PSNR (peak signal-to-noise ratio) compared to Wiener deconvolution (Thakur & Datar, 2014; Al-Taweel et al., 2015). Although PSF estimation can be computationally intensive, it remains critical for enhancing image quality (Liu et al., 2024).

This study also employed thresholding techniques on fluorescent images, enabling more precise quantification. Both global and local contrast enhancement techniques were applied to improve image clarity. While global histogram equalization enhanced overall image contrast, adaptive histogram equalization proved more effective in emphasizing specific image details, particularly within localized regions such as the nuclei. However, it is important to acknowledge that local histogram equalization may introduce unwanted artifacts, leading to potential data loss (Somal, 2020). Given that our study focused on β-catenin within nuclei, adaptive histogram equalization was better suited to our needs than global methods.

While our deconvolution algorithms were successful in improving the clarity of β-catenin's nuclear localization, several limitations need to be addressed. The algorithms implemented in MATLAB and Python provided useful insights, but potential errors remain. These include challenges with accurately estimating the PSF, which can introduce inaccuracies in deconvolution. Additionally, variations in β-catenin intensity across time points, especially in post-deconvolution images, may complicate quantification efforts. Future studies could improve upon our work by incorporating advanced blind deconvolution techniques that more accurately estimate the PSF, potentially using adaptive algorithms like the enhanced Lucy Richardson method.

Looking forward, future research could explore automating the deconvolution process to minimize errors

and improve accuracy. Employing machine learning-based approaches to PSF estimation could also enhance precision, especially when working with highly variable or noisy data. Moreover, the integration of auto-threshold methods could further refine our analysis, ensuring more consistent and reproducible results across different imaging conditions. Ultimately, these advancements could bolster the utility of β-catenin as a reliable marker for tracking cancer progression, while our algorithms provide a valuable tool for visualizing and quantifying these changes with greater precision.

5. CONCLUSION

This study sought to quantify this critical process by using deconvolution techniques to reduce out-of-focus blur from WFFM images, offering a cost-effective approach for detailed analysis. By testing various algorithms across two different platforms, comparable results were successfully achieved, demonstrating the reliability of the method. This study has significant practical implications, particularly for laboratories with limited financial resources. It provides a cost-effective alternative to expensive confocal and super-resolution microscopy, enabling high-resolution and accurate spatial localization of fluorescently labeled molecules.

ACKNOWLEDGMENTS

The authors would like to thank the Department of Biotechnology, Government of India for providing grant in the form of Indo-Australian Career Boosting Gold Fellowship (IACBGF). The authors would like to thank the School of Biotechnology and Biomolecular Sciences, University of New South Wales, Sydney, Australia and the Centre for Biomaterials Cellular and Molecular Theranostics, VIT, University, Vellore, India where the experimental and analytical research was carried out respectively.

AUTHOR CONTRIBUTIONS

R.N. and A.K. contributed to Manuscript preparation, Data acquisition, Data analysis and interpretation. C.N. and N.W. contributed to Study design and carrying out the experiments. P.S. contributed to Statistical analysis, and for manuscript reviewing and editing. R.K.D. carried the experiments, helped in data acquisition, conceptualized the study, and edited the manuscript.

REFERENCES

Al-Taweel, R. S. H., Daway, H. G., & Kahmees, M. H. (2015). Deblurring average blur by using adaptive Lucy Richardson. *Journal of College of Education*, *5*(2015), 75–90.

Bai, H., Che, B., Zhao, T., Zhao, W., Wang, K., Zhang, C., & Bai, J. (2022). Feature extraction of 3T3 fibroblast microtubule based on discrete wavelet transform and Lucy-Richardson deconvolution methods. *Micromachines*, *13*(6), Article 824. https://doi.org/10.3390/mi13060824

Bruce, M. A., & Butte, M. J. (2013). Real-time GPU-based 3D deconvolution. *Optics Express*, *21*(4), 4766–4773. https://doi.org/10.1364/OE.21.004766

Chakraborti, S., Karmakar, A., Guha, R., Ngan, C., Das, R. K., & Whitaker, N. (2023). Induction of epithelial to mesenchymal transition in HPV16 E6/E7 oncogene transfected C33A cell line. *Tissue and Cell*, *82*, Article 102041. https://doi.org/10.1016/j.tice.2023.102041

Disoma, C., Zhou, Y., Li, S., Peng, J., & Xia, Z. (2022). Wnt/β-catenin signaling in colorectal cancer: Is therapeutic targeting even possible? *Biochimie*, *195*, 39–53. https://doi.org/10.1016/j.biochi.2022.01.009

Grimm, J. B., & Lavis, L. D. (2022). Caveat fluorophore: An insiders' guide to small-molecule fluorescent labels. *Nature Methods*, *19*, 149–158. https://doi.org/10.1038/s41592-021-01338-6

Hasan, H. K. (2016). *Restoration of digital images using an iterative Tikhonov-Miller filter* [Master's thesis, Al-Nahrain University]. Al-Nahrain University. https://www.nahrainuniv.edu.iq/en/node/6053

He, Z., Wang, H., Li, Y., Zhang, Z., Zhang, Y., Bi, H., & He, Y. (2021). A deconvolutional reconstruction method based on Lucy–Richardson algorithm for joint scanning laser thermography. *IEEE Transactions on Instrumentation and Measurement*, *70*, Article 4501508. https://doi.org/10.1109/TIM.2020.3034967

Hickey, S. M., Ung, B., Bader, C., Brooks, R., Lazniewska, J., Johnson, I. R. D., Sorvina, A., Logan, J., Martini, C., Moore, C. R., Karageorgos, L., Sweetman, M. J., & Brooks, D. A. (2022). Fluorescence microscopy—An outline of hardware, biological handling, and fluorophore considerations. *Cells*, *11*(1), Article 35. https://doi.org/10.3390/cells11010035

Hojjatoleslami, S. A., Avanaki, M. R. N., & Podoleanu, A. G. (2013). Image quality improvement in optical coherence tomography using Lucy-Richardson deconvolution algorithm. *Applied Optics*, *52*(23), 5663–5670. https://doi.org/10.1364/AO.52.005663

Kanthan, M. R., & Sujatha, S. N. (2016, December 15–17). *Blur removal using blind deconvolution and gradient energy* [Conference session]. 2016 IEEE International Conference on Computational Intelligence and Computing Research (ICCIC), Chennai, India. https://doi.org/10.1109/ICCIC.2016.7919556

Kaszak, I., Witkowska-Piłaszewicz, O., Niewiadomska, Z., Dworecka-Kaszak, B., Ngosa Toka, F., & Jurka, P. (2020). Role of cadherins in cancer—A review. *International Journal of Molecular Sciences*, *21*(20), Article 7624. https://doi.org/10.3390/ijms21207624

Kaur, H., & Kaur, M. (2016). A hybrid approach for blur detection using Naïve Bayes nearest neighbor classifier. *International Journal of Information Technology and Computer Science (IJITCS)*, *8*(12), 75–82. https://doi.org/10.5815/ijitcs.2016.12.09

Khan, S. A., Hussain, S., & Yang, S. (2020). Contrast enhancement of low-contrast medical images using modified contrast limited adaptive histogram equalization. *Journal of Medical Imaging and Health Informatics*, *10*(8), 1795–1803. https://doi.org/10.1166/jmihi.2020.3196

Kim, B. (2021). DVDeconv: An open-source MATLAB toolbox for depth-variant asymmetric deconvolution of fluorescence micrographs. *Cells*, *10*(2), Article 397. https://doi.org/10.3390/cells10020397

Kumar, A., Kumar, P., & Srivastava, S. (2022). A skewness reformed complex diffusion based unsharp masking for

the restoration and enhancement of Poisson noise corrupted mammograms. *Biomedical Signal Processing and Control*, *73*, Article 103421. https://doi.org/10.1016/j.bspc.2021.103421

Lambert, T. J., & Waters, J. C. (2017). Navigating challenges in the application of superresolution microscopy. *Journal of Cell Biology*, *216*(1), 53–63. https://doi.org/10.1083/jcb.201610011

Lau, A., Fétick, R. J. L., Neichel, B., Beltramo-Martin, O., & Fusco, T. (2023). Improved prior for adaptive optics point spread function estimation from science images: Application for deconvolution. *Astronomy & Astrophysics*, *673*, Article A72. https://doi.org/10.1051/0004-6361/202245471

Liu, C., Sun, M., Wu, W., Dai, N., Guo, M., Wei, Y., Wu, X., & Fu, H. (2024). Enhancing the resolution of three-dimensional migration images based on space-variant point spread function deconvolution. *Geophysical Prospecting*, *72*(5), 1672–1697. https://doi.org/10.1111/1365-2478.13477

Perrone, F., Bertolotti, A., Montemurro, G., Paolini, B., Pierotti, M. A., & Colecchia, M. (2014). Frequent mutation and nuclear localization of β-catenin in Sertoli cell tumors of the testis. *The American Journal of Surgical Pathology*, *38*(1), 66–71. https://doi.org/10.1097/PAS.0b013e31829cdbc6

Pietzsch, T., Preibisch, S., Tomančák, P., & Saalfeld, S. (2012). ImgLib2—generic image processing in Java. *Bioinformatics*, *28*(22), 3009–3011. https://doi.org/10.1093/bioinformatics/bts543

Pushpa, N. B., Patra, A., & Ravi, K. S. (2023). Advances in microscopy and its applications with special reference to fluorescence microscope: An overview. In E. A. Meguid, P. L. Mishall, H. L. Nation, & P. M. Rea (Eds.), *Biomedical visualisation* (pp. 3–17). Springer. https://doi.org/10.1007/978-3-031-26462-7_1

Ramos-García, P., & González-Moles, M. Á. (2022). Prognostic and clinicopathological significance of the aberrant expression of β-catenin in oral squamous cell carcinoma: A systematic review and meta-analysis. *Cancers*, *14*(3), Article 479. https://doi.org/10.3390/cancers14030479

Sage, D., Donati, L., Soulez, F., Fortun, D., Schmit, G., Seitz, A., Guiet, R., Vonesch, C., & Unser, M. (2017). DeconvolutionLab2: An open-source software for deconvolution microscopy. *Methods*, *115*, 28–41. https://doi.org/10.1016/j.ymeth.2016.12.015

Satish, P., Srikantaswamy, M., & Ramaswamy, N. K. (2020). A comprehensive review of blind deconvolution techniques for image deblurring. *Traitement du Signal*, *37*(3), 527–539. https://doi.org/10.18280/ts.370321

Schneider, C. A., Rasband, W. S., & Eliceiri, K. W. (2012). NIH Image to ImageJ: 25 years of image analysis. *Nature Methods*, *9*(7), 671–675. https://doi.org/10.1038/nmeth.2089

Shi, R., Jin, C., Xie, H., Zhang, Y., Li, X., Dai, Q., & Kong, L. (2019). Multi-plane, wide-field fluorescent microscopy for biodynamic imaging *in vivo*. *Biomedical Optics Express*, *10*(12), 6625–6635. https://doi.org/10.1364/BOE.10.006625

Sidhu, R. K., Sachdeva, J., & Katoch, D. (2023). Segmentation of retinal blood vessels by a novel hybrid technique—Principal component analysis (PCA) and contrast limited adaptive histogram equalization (CLAHE). *Microvascular Research*, *148*, Article 104477. https://doi.org/10.1016/j.mvr.2023.104477

Somal, S. (2020). Image enhancement using local and global histogram equalization technique and their comparison. In A. K. Luhach, J. A. Kosa, R. C. Poonia, X.-Z. Gao, & D. Singh (Eds.), *First International Conference on Sustainable Technologies for Computational Intelligence (ICTSCI 2019). Advances in intelligent systems and computing, Vol. 1045* (pp. 739–753). Springer. https://doi.org/10.1007/978-981-15-0029-9_58

Thakur, M., & Datar, S. (2014). Image restoration based on deconvolution by Richardson Lucy algorithm. *International Journal of Engineering Trends and Technology*, *14*(2), 161–165. https://doi.org/10.14445/22315381/IJETT-V14P232

Valli, J., Garcia-Burgos, A., Rooney, L. M., de Melo e Oliveira, B. V., Duncan, R. R., & Rickman, C. (2021). Seeing beyond the limit: A guide to choosing the right super-resolution microscopy technique. *Journal of Biological Chemistry*, *297*(1), Article 100791. https://doi.org/10.1016/j.jbc.2021.100791

Wu, X., & Hammer, J. A. (2021). ZEISS Airyscan: Optimizing usage for fast, gentle, super-resolution imaging. In J. Brzostowski & H. Sohn (Eds.), *Confocal Microscopy: Methods and Protocols* (pp. 111–130). Humana Press. https://doi.org/10.1007/978-1-0716-1402-0_5

Wu, Y., Han, X., Su, Y., Glidewell, M., Daniels, J. S., Liu, J., Sengupta, T., Rey-Suarez, I., Fischer, R., Patel, A., Combs, C., Sun, J., Wu, X., Christensen, R., Smith, C., Bao, L., Sun, Y., Duncan, L. H., Chen, J., . . . Shroff, H. (2021). Multiview confocal super-resolution microscopy. *Nature*, *600*, 279–284. https://doi.org/10.1038/s41586-021-04110-0

Xu, C., Liu, F., Xiang, G., Cao, L., Wang, S., Liu, J., Meng, Q., Xu, D., Lv, S., Jiao, J., & Niu, Y. (2019). β-Catenin nuclear localization positively feeds back on EGF/EGFR-attenuated AJAP1 expression in breast cancer. *Journal of Experimental & Clinical Cancer Research*, *38*(1), Article 238. https://doi.org/10.1186/s13046-019-1252-6

Yadav, S., Jain, C., & Chugh, A. (2016). Evaluation of image deblurring techniques. *International Journal of Computer Applications*, *139*(12), 32–36. https://doi.org/10.5120/IJCA2016909492